Energy 278 (2023) 127957

Contents lists available at ScienceDirect

Energy

journal homepage: www.elsevier.com/locate/energy

Suitability of wave energy converters in northwestern Spain under the near future winter wave climate

B. Arguilé-Pérez [a,*], A.S. Ribeiro [a,b], X. Costoya [a], M. deCastro [a], M. Gómez-Gesteira [a]

[a] Centro de Investigación Mariña, Universidade de Vigo, Environmental Physics Laboratory (EPhysLab), Campus da Auga, 32004, Ourense, Spain
[b] CESAM, Physics Department, University of Aveiro, 3810-193, Aveiro, Portugal

ARTICLE INFO

Handling Editor: G Iglesias

Keywords:
Wave energy
Wave energy converters (WECs)
Climate change
Galician coast
WaveWatch III
SWAN

ABSTRACT

Marine renewable energies can play a key role by reducing the dependency on fossil fuels and, therefore, mitigating climate change. Among them, it is expected that wave energy will experience rapid growth in the upcoming decades. Thus, it is important to know how wave climate will change and how suitable the wave energy converters (WECs) will be to the new wave conditions. This paper aims to evaluate the capability of four different WECs—a WaveRoller type device (WRTD), Atargis, AquaBuoy and RM5—to extract wave energy on the Northwest coast of Spain (NWCS). The analysis was performed using the high-resolution wave data obtained from the Simulating Waves Nearshore (SWAN) model over the near future winters (2026–2045). The energy output (P_E), the power load factor (ε), the normalized capture width (NC_w) and the operational time (OT) were analyzed. According to these parameters, among the devices that work for intermediate-deep waters, Atargis would be the best option (P_E=1400 ± 56 kW, ε =55.4 ± 2.2%, NC_w=35.5 ± 4.1% and OT =84.5 ± 3.3%). The WRTD would also be a good option for shallow nearshore areas with P_E=427 ± 248 kW, ε =12.8 ± 7.4%, NC_w = 48.9 ± 9.6% and OT = 88.7 ± 18.9%. A combination of Atargis and WRTDs is proposed to make up the future wave energy farms on the NWCS.

1. Introduction

Wave energy is one of the most abundant and constant renewable energy sources since waves are able to propagate thousands of miles with minimal energy loss, even if the wind is not blowing [1]. The global energy potential of waves is estimated to be between 29,500 and 32,000 TW h/year [2], so it is interesting to consider harnessing this energy source to achieve the energy targets of the United Nations 2030 Agenda for sustainable development. Wave energy converters (WECs) are still in the development stages, so the wave energy resource is not yet being commercially exploited. Therefore, it is necessary to increase the efficiency and reduce the costs of these technologies to gain industry recognition as an alternative energy source. Due to the goal of carbon-free energy worldwide and a need to diversify the mix of renewable energies, wave energy extraction can become an appropriate complement to existing and more mature renewable energy technologies such as offshore wind farms in the coming decades [2]. In order to make good planning of the renewable energy mix, it is necessary to study the impact of climate change on wave power in the near future.

Few studies analyze the future wave energy resource compared with other renewable resources such as wind. Most studies just analyze future wave climate (see, for example [3–16]) rather than analyzing the wave power itself because wave energy resource depends on the wave significant height and period. Thus, for example [13], analyzed the variation of the wave power in the North Atlantic basin and the Mediterranean Sea under three different Representative Concentration Pathway (RCP) greenhouse concentration scenarios (RCP2.6, RCP4.5 and RECP8.5) for three periods (2010–2039, 2040–2069 and 2070–2099). They found a clear decrease in wave energy, except for the Norwegian coast. Rusu et al. [17,18] investigated the impact of climate change on wave energy in the Black Sea and found a high seasonal variability of wave energy under future conditions (for 2021–2050 and 2071–2100, respectively) under the RCP4.5 and RCP8.5 scenarios. Alizadeh et al. [19] did not find a significant change in annual wave energy in the Caspian Sea at the end of the century (2081–2100) under the SSP2-4.5 and SSP5-8.5 scenarios, but a slightly decreasing trend in autumn and winter. Goharnejad et al. [20] also found no clear trend in wave power in the Persian Gulf in 2070–2099 under the RCP4.5 and

* Corresponding author.
E-mail addresses: beatriz.arguile.perez@uvigo.es (B. Arguilé-Pérez), americosribeiro@ua.pt (A.S. Ribeiro), xurxocostoya@uvigo.es (X. Costoya), mdecastro@uvigo.es (M. deCastro), mggesteira@uvigo.es (M. Gómez-Gesteira).

https://doi.org/10.1016/j.energy.2023.127957
Received 8 November 2022; Received in revised form 14 April 2023; Accepted 26 May 2023
Available online 29 May 2023

RCP8.5 scenarios, because it did not show a seasonal trend. However, they found a descending trend in winter. Ribeiro et al. [21] observed a decrease in mean wave energy and an increase in its seasonal variability in the west of the Atlantic Arc in the far future (2081–2100) under the RCP8.5 scenario.

Few studies evaluated the WECs performance in obtaining energy from waves in the future decades. Reeve et al. [22] found that the impact of climate change would negatively affect energy generation by Pelamis (attenuator type of WEC) in the southwest UK because the energy output that could be obtained would decrease by 2–3% at the end of the century (2061–2100) under the A1B and B1 scenarios. Sierra et al. [23] analyzed the amount of electric energy delivered by two types of WECs (Pelamis, and Wave Dragon — overtopping type) under future conditions (2081–2100, RCP4.5 and RCP8.5) in a context of climate change around the island of Menorca (NW Mediterranean Sea), as well as its annual and seasonal variability. In that study, they found that the wave energy output shows future reductions between 0 and 5%. In this regard, Ribeiro et al. [1] also found a decrease in the future energy output that could be obtained with Pelamis and AquaBuoy (point absorber type of WEC) along the west coast of the Iberian Peninsula under the RCP8.5 and 2081–2100. Note that while Reeve et al. [22] and Sierra et al. [23] focused only on studying the energy yield, Ribeiro et al. [1] also addressed the WECs efficiency using two additional parameters: the power load factor and the capture width. The lack of research on how climate change will affect the energy production and efficiency of WECs may be because their Technology Readiness Level (TRL) is still low compared to, for example, wind turbines. Furthermore, there is no WEC technology that is clearly more efficient than the rest of WECs. Therefore, taking into account that each WEC has its characteristics (geometry, size, power take-off system), more research is required on the performance of different WECs under future wave climatic conditions.

The Galician coast (NW Spain) is strongly influenced by low-pressure systems in the mid-Atlantic Ocean and the periodic passage of storms which may intensify the sea states. The Northwest Coast of Galicia is the region with the highest wave energy in Spain —and one of the highest in Europe—[24–26], with a mean annual power between 40 and 45 kWm^{-1} [27]. This feature is due to its privileged location and northwest orientation, which benefits from the westerly winds and a swell component most of the year (more than 78%) [28]. Generally, the highest wave heights are obtained during the winter months [29], when the average power of the waves in Galicia is estimated at 75 kWm^{-1} [30].

Previous research ([31]), highlights that combining different types of energy is a way of stabilizing the energy mix. During winter, photovoltaic solar energy is at its minimum value and must be compensated with other renewable energies (mainly wind and wave energy). That is why it is relevant to know the capacity of different WECs to extract energy during that period of the year.

This paper aims to assess how different WECs can fit near future (2026–2045) wave conditions and their efficiency to extract energy. The study will be carried out on the Northwest Coast of Spain in winter conditions because it is when the sea states are more energetic. The RCP8.5 scenario was chosen because it is helpful for assessing climate risk from a short-to medium-term perspective, as noted by Ref. [32]. The energy output, the time during which WECs remain in operation (operational time), the power load factor and the normalized capture width of every device will be analyzed under near future wave conditions.

2. Data, wave models and methodology

2.1. Study region, data and wave models

The study has focused on the area with the greatest wave energy potential in Spain, the Northwest Coast of Galicia [24]. Fig. 1 depicts the region under study. Fig. 1a shows an amplification of the study area, where the North Atlantic Arc is shown. Fig. 1b represents the study area itself.

A series of steps were followed to obtain high-resolution wave climate data off the Northwest coast of Spain that would allow us to analyze the suitability of WECs for energy extraction in the near future (Fig. 2). Thus, the identification of the best GCM to describe the wave climate during winters was performed by determining the RMSE and Bias to the 8 GCMs [21,33] available at the Commonwealth Scientific

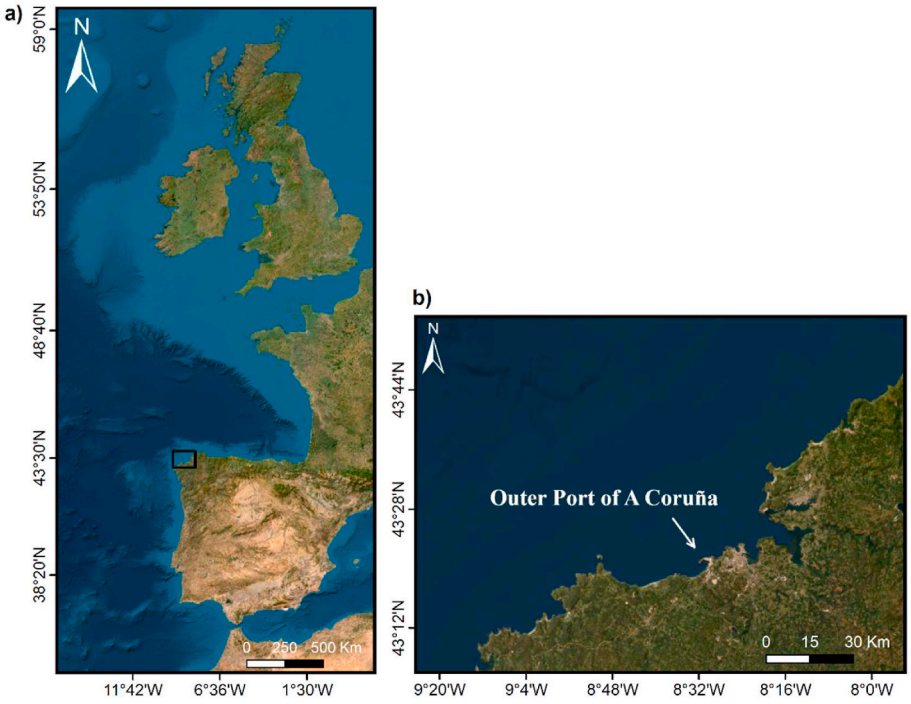

Fig. 1. Atlantic Arc area (a) and study area (b).

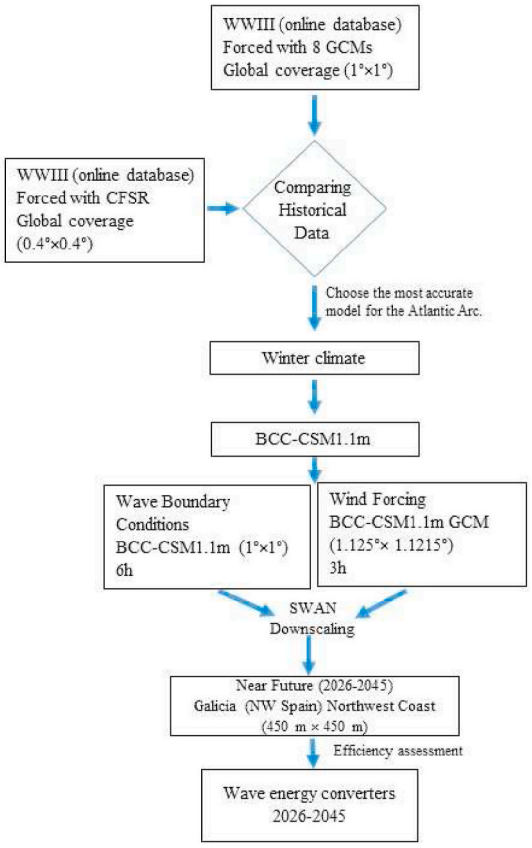

Fig. 2. Procedure sketch to obtain high resolution data of wave climate.

and Industrial Research Organisation (CSIRO) database (http://data-cbr.csiro.au/thredds/catalog/catch_all/CMAR_CAWCR-Wave_archive/Global_wave_projections/catalog.html [34]), taking into account the significant wave height (H_s) and wave peak period (T_p), which is observed during the winter months (December, January and February) for the period between 1979 and 2005. Ribeiro et al. [33] analyzed the RMSE and Bias indicators of the 8 GCMs, which showed that the BCC-CSM1.1 GCM represents the best GCM to reproduce the study area's winter wave climate.

The BCC-CSM1.1 GCM has a temporal and spatial resolution of 6 h and 1° × 1°, respectively. This coarse resolution is not suitable for performing a WEC assessment, which is requiring to perform dynamic downscaling. Thus, the third-generation spectral wave model Simulating Waves Nearshore (SWAN), integrated into the Delft3D-WAVE module [35], was used by applying a similar approach to Refs. [21,33]. A nested model implementation was adopted, covering the Galician coast and increasing resolution towards the study area on the Northwest coast of Spain (Fig. 3), using the identified GCM as an open ocean boundary (D0, Fig. 3a). Table 1 summarizes the characteristics of each domain. The bathymetry was generated from the General Bathymetry Chart of the Oceans [36]. The ocean forcing was introduced at each grid node intersection between domains D0 and D1. The atmospheric variables were also considered by using the BCC-CSM1-1-m GCM (https://data.ceda.ac.uk/badc/cmip5/data/cmip5/output1/BCC/bcc-csm1-1-m/rcp85/3hr/atmos/3hr/r1i1p1/v20130411) [37]). Two variables have been chosen as atmospheric data: eastward near-surface wind speed and northward near-surface wind speed. The temporal and spatial resolutions are 3-h and 1.125° × 1.1215°, respectively. As previously mentioned in the introduction section, on the Northwest coast of Galicia, the swell component is predominant most of the year [28] with a dominant wave direction from the northwest. For this reason, most waves are derived from swell and can be reasonably simulated using low-resolution wind data, as Santos et al. showed in Ref. [38] by obtaining overlap function values greater than 70% when compared GCMs with coastal buoys and inland locations. The future period selected was 2026–2045. As simulations were carried out during the winter months (December, January and February), November was used as a model spin-up for each winter.

The recommendations for a stage 1 (reconnaissance) model of the technical specification IEC-TS 62600-101 have been followed. Physical parameters such as triads, bottom friction, depth-induced breaking and quadruplets were included. The spatial and temporal resolution of the wave results in the area under scope (D4 domain, Fig. 3b) is 450 m × 450 m and 1 h, respectively. The wave spectrum consists of 25

Table 1
Characteristics of the numerical domains applied in the downscaling.

Domain	Extension	Spatial resolution
D0	13.54 °W, 34.54 °N – 0.45 °E, 50.54 °N	1° × 1°
D1	12.54 °W, 35.54 °N – 0.55 °W, 49.54 °N	1/3° × 1/3°
D2	10.89 °W, 36.54 °N – 0.55 °W, 47.88 °N	1/9° × 1/9°
D3	Portuguese, Spanish and French Atlantic Coast 38.80 °N – 47.87 °N	1/27° × 1/27°
D4	Northwest Coast of Galicia, 8.84 °W, 43.06 °N – 8.18 °W, 43.76 °N	450 m × 450 m

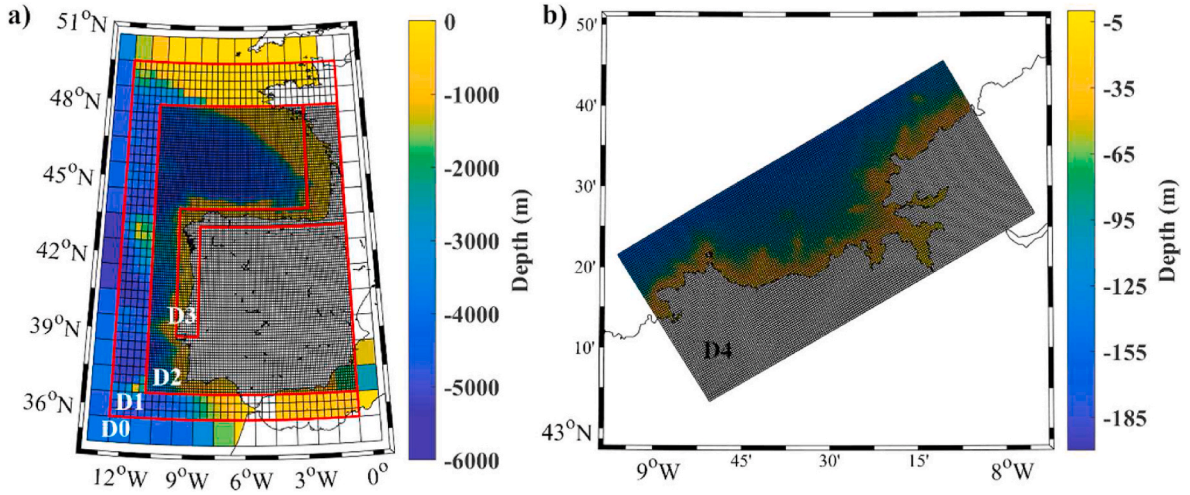

Fig. 3. Numerical domains and bathymetry used in the SWAN downscaling of the BCC-CSM1.1 m GCM (a, b) and the study region (b). Only the boundaries of domain D3 have been plotted to ensure proper visualization.

frequencies (from 0.04 Hz to 1 Hz) and 36 directional bands.

2.2. Wave power resource

The wave power resource (*WP*) is defined as the amount of energy flux per unit length of the wavefront transmitted in the direction of the wave propagation [39]. In that way, the most energetic waves are linked to high values of *WP*. The *WP* is expressed in kWm^{-1}, and it is mathematically defined by equation (1):

$$WP = \alpha \frac{\rho g^2}{64\pi} H_s^2 T_p \quad (1)$$

where ρ is the density of seawater (considered as 1025 kgm^{-3}), g is the gravitational acceleration, H_s is the significant wave height, T_p is the

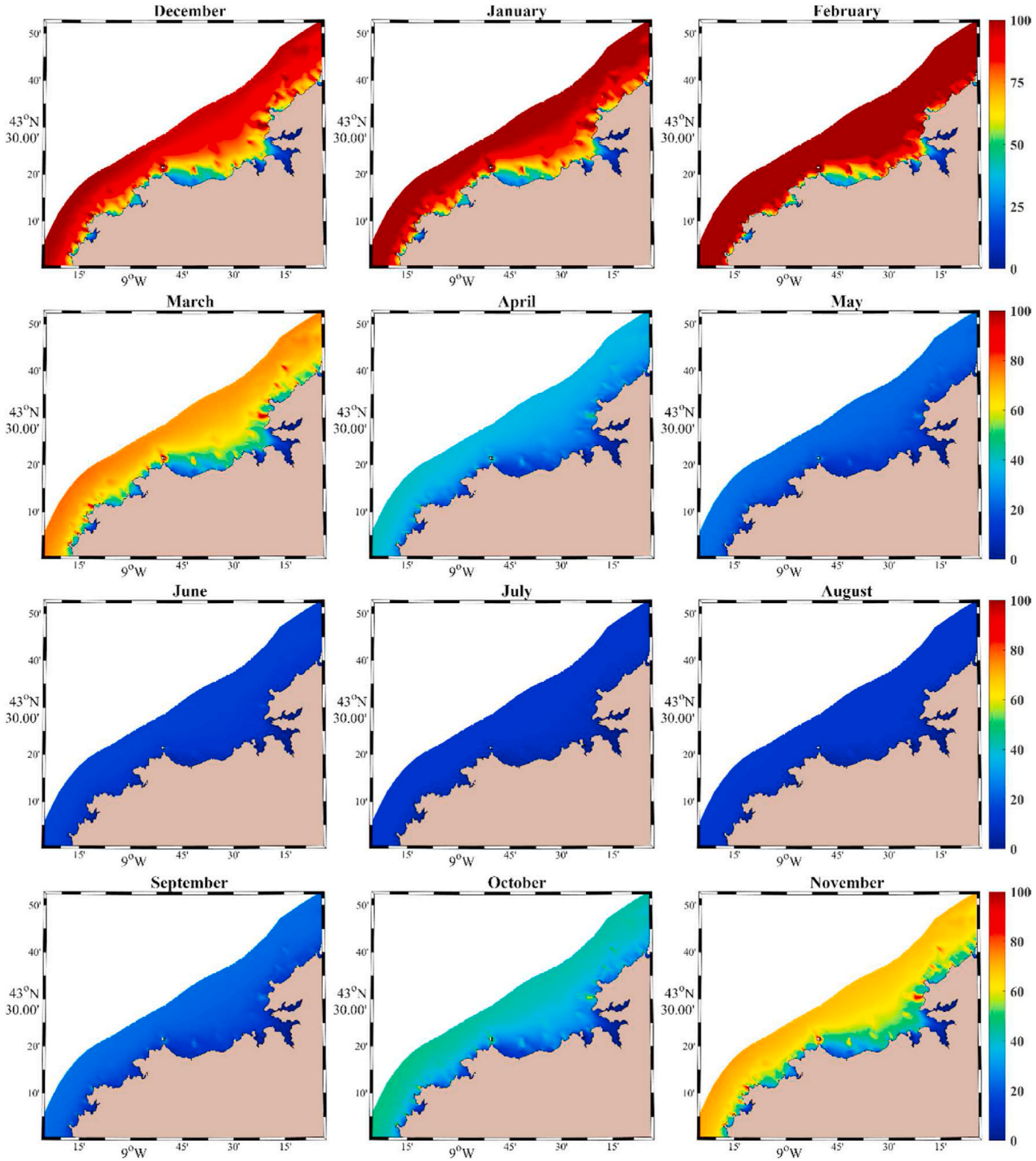

Fig. 4. Monthly-averaged wave power resource (*WP*, kWm^{-1}) for the period 2014–2021, considering the same data as in Ref. [27].

wave peak period, and α is a factor related to the shape of the wave spectrum. A conservative value of $\alpha = 0.9$ was assumed in the present work similar to previous studies [40,41], which is equivalent to assuming a standard JONSWAP spectrum with a peak enhancement of $\gamma = 3.3$ [1]. See Ref. [42] for more details.

For the area under study, the winter months (December, January and February) have shown to be the most energetic, with a *WP* exceeding 90−100 kWm^{-1} for the period 2014–2021, being February the most energetic month (Fig. 4). Thus, the winter season was selected as representative of the most energetic period to study the WECs' behavior.

2.3. WEC devices and wave climate characterization

Four WECs were considered in this study: a WaveRoller type device (see Fig. 3 in Ref. [43]), Atargis (see Fig. 1 in Ref. [44]), AquaBuoy (see Fig. 8 in Ref. [43]) and RM5 (see Fig. 1 in Ref. [45]). WaveRoller is a bottom-fixed Oscillating Wave Surge Converter (OWSC) suitable for shallow water depths (8−20 m) [45–47]. For reasons of the manufacturer's confidentiality, a similar device was considered in the present work (WRTD from now on). Atargis is a Cycloidal Wave Energy Converter (CycWEC) designed to operate at intermediate water depths (+40 m) [44]. The point absorber type device AquaBuoy and the Floating Oscillating Wave Surge Converter (FOWSC) RM5 are offshore devices suitable for working in deep waters (+50 m) [48] (see Table 2). Each WEC is designed to operate not only in a specific depth range but also in specific H_s and T_p. The manufacturer provides information about the optimum operating intervals for H_s and T_p, represented on their power matrix. The power matrix shows the electric power produced by the device according to the sea state (H_s, T_p), i.e. each WEC obtains more energy with some sea states than with others. The power matrices for the four WECs considered are shown in the Appendix. There, it can be seen that the WRTD (Table A1) operates at a wide range of H_s (1 m−7 m) and T_p (4 s−16 s). It produces more energy for sea states with H_s values from 6 to 7 m and T_p values from 8 to 12 s. This means that the WRTD device is suitable for areas with high waves with intermediate periods. Atargis (Table A2) has a more limitant H_s and T_p ranges of operation ($\sim 0.7\ m \leq H_s \leq \sim 4.5\ m$, $4.5\ s \leq T_p \leq 15.5$). It is able to produce its maximum energy at lower H_s and T_p values ($3.0\ m \leq H_s \leq 4.5\ m$, $6.5\ s \leq T_p \leq 13.5$), being suitable for lower waves. AquaBuoy (Table A3) also shows a more restricted H_s range ($1\ m \leq H_s \leq 5.5\ m$) and a wider T_p range ($6\ s \leq T_p \leq 17\ s$). It is more suitable for areas with higher waves than Atargis (where H_s varies from 4.5 m to 5.5 m) and the same period range to the WRTD ($8\ s \leq T_p \leq 12\ s$). Finally, RM5 (Table A4) also has a limited H_s range ($0.75\ m \leq H_s \leq 5.75\ m$) but a vast T_p range ($5.2\ s \leq T_p \leq 20.3\ s$). It produces its maximum energy in those areas where H_s varies from 4.5 m to 6 m and T_p from 5 s to 15 s.

Power matrices are related to the power take-off (PTO) system of the WEC. For example, as pointed by Ahamed et al. in Ref. [43], WECs with an hydraulic motor PTO system like the WRTD or RM5 are able to generate a big amount of energy from the low frequency waves (large periods). Regarding the amount of power generated, it can be seen that Atargis is able to produce ten times more power than AquaBuoy. In spite of being both based on hydro turbine PTO system, Atargis is also ten time larger than AquaBuoy, and this can be the reason why Atargis can extract more energy than AquaBuoy. More information about these WECs can be found in Ref. [49], [56–58], [55].

The probability of occurrence of each sea state has been calculated to characterize the wave climate. This probability ($\overline{p}$ij expressed in percentage) is addressed by separating the range of simulated values of H_s and T_p in bins, and then by counting the number of sea states (N_{ij}) that correspond to each bin (i, j), considering the whole data series for the near future period (2026–2045) and the study area. Later, N_{ij} is divided by the total number of sea states (N) and multiplied by 100.

$$\overline{p}_{ij}(\%) = 100 \cdot \frac{N_{ij}}{N} \tag{2}$$

Finally, the probability of occurrence of the sea states and the power matrix are compared graphically to visualize how well a WEC suits the winter wave climate.

2.4. Electric power output

The total electric power output that a particular WEC can extract depends on the *WP* resource available and the performance of the WEC in extracting the energy. The performance of every WEC is related to the power matrix, which depends on the WEC's geometric shape, size, and PTO system parameters. The expected average electric power (P_E, in kW) that can be extracted with a particular WEC at a certain point (pixel) of the study area is expressed by equation (3):

$$P_E = \frac{1}{100} \sum_{i=1}^{n_T} \sum_{j=1}^{n_H} p_{ij} P_{ij} \tag{3}$$

where P_{ij} is the electric power obtained from an element (i, j) of the power matrix of a particular WEC, p_{ij} is the probability of occurrence of a given sea state for every pixel in percentage, and n_T and n_H are the numbers of wave peak period and significant wave height bins considered, respectively.

2.5. Suitability parameters

2.5.1. Power load factor and normalized capture width

The power load factor (ε) is defined as the relation between P_E and the maximum power (P_{max}) that the device can produce, computed as the maximum value of the power matrix (see equation (4)). If the device is well-fitted to the wave climate, P_E will be close to P_{max}, obtaining a high ε.

$$\varepsilon\ (\%) = 100 \cdot \frac{P_E}{P_{max}} \tag{4}$$

The normalized capture width (NC_w) is the power generated by the WEC (P_E) per unit of length (L) with respect to the available wave power resource (*WP*), estimating the efficiency of the WEC in converting the wave energy resource into electricity. This variable is defined in equation (5), being L a value shown in Table 2.

Table 2
Characteristics of WECs, including: structure, type, wave energy mode, power take off system (PTO), maximum electric power, depth range for the WECs installation and WEC length opposite to the wave. A picture of these WECs can be found in the referenced literature.

Name	Structure	Classification	Energy mode	PTO	P_{max} (kW)	Depth (m)	L (m)	References
WRTD	Semi-submerged two-body structure	Oscillating Wave Surge Converter (OWSC)	Surge	Hydraulic motor	3332	8–20	26	[43,46,49]
Atargis	Completely submerged twin hydrofoil-based structure	Cycloidal Wave Energy Converter (CycWEC)	Heave and Surge	Hydro turbine	2530	40–100	60	[43,44,50,51]
AquaBuoy	Two-body floating system	Point absorber	Heave	Hydro turbine	250	50–100	6	[43,52–54]
RM5	Semi-submerged two-body structure with moorings	Floating Oscillating Wave Surge Converter (FOWSC)	Surge	Hydraulic motor	360	50–100	25	[55]

$$NC_w\ (\%) = 100 \cdot \frac{P_E}{WP \cdot L} \tag{5}$$

2.5.2. Operational time

The operational time for a specific device is defined as the percentage of time at which a WEC can operate. The concepts of operational time and downtime are opposites as described in previous research [22,59]. In particular [22], only considered the H_s influence in determining the time range in which the device is not working. In the present study, the T_p is also taken into account. Thus, the operational time (OT, in percentage, from now on) is computed as the sum of the probability of occurrence of each sea state in a certain pixel, considering exclusively the H_s and T_p bins for which the power matrix has non-zero values (see equation (6)).

$$OT\ (\%) = \sum_{i=1}^{n_T} \sum_{j=1}^{n_H} p_{ij}, \forall i,j \ \Big| \ P_{ij} \neq 0 \tag{6}$$

Note that all these three suitability parameters depend on the power matrix of the different devices, in such way that to attain efficient devices, the very energetic sea states observed in winter should match the characteristics of the WECs.

2.6. Statistical errors

The average value of each suitability parameter previously defined will be calculated accompanied by its standard deviation, computed using equation (7).

$$\sigma = \sqrt{\frac{1}{M-1} \sum_{m=1}^{M} (x_m - \bar{x})^2} \tag{7}$$

where M is the total number of pixels, x_m is the value of the suitability parameter in the pixel m and $\bar{x}$ is the average value of the suitability parameter.

3. Results

3.1. WEC suitability under future wave climate

The probability of occurrence of every winter sea state for different depths of the study area from 2026 to 2045 and the WECs power matrix for each water depth range have been plotted together in a bivariate diagram (Fig. 5). Red (blue) color indicates the most (least) probable sea states.

Regarding the probabilities of occurrence of sea states in shallow waters (Fig. 5a), the most likely waves (probability ~1.6−2%) show a H_s of around 1−2 m and a T_p of 10–12 s. For intermediate and deep waters (Fig. 5b–d), the most likely waves will have a H_s between 2 and 4 m and T_p of 9–13 s.

Considering the power matrices, the WRTD (Fig. 5a) can produce a maximum energy power (3332 kW) for waves with H_s between 6 and 7.5 m, which will not occur in the shallow waters in the region . Therefore, a low overlap between the WRTD's power matrix and the shallow waters sea states can be observed. The device can only generate a maximum power of around 100−240 kW for the most frequent sea states observed in shallow waters.

Atargis is a device well suited for the future wave climate of the

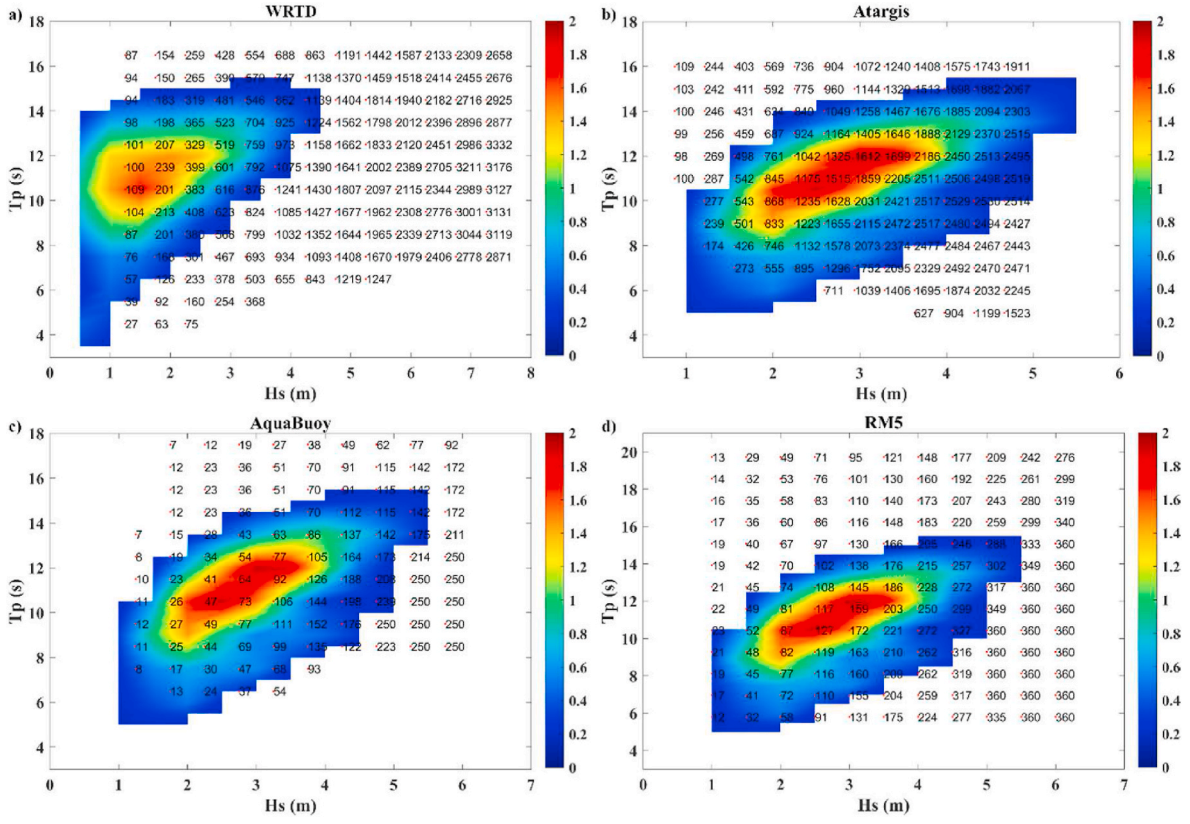

Fig. 5. Bivariate distributions of winter sea state probability of occurrence (%, colors) for different depths of the study area for the period 2026–2045 and the power matrix of the suitable WEC (numbers, in kW) for its optimum operational water depth range. The red dot that accompanies the element of the power matrix indicates the center of the interval of each sea state to which each element of the power matrix refers.

region. The most likely sea states show powers of 1200–1900 kW compared to the maximum 2530 kW obtained for H_s of 3–4.5 m and T_p of 6.5–13.5 s (Fig. 5b). A moderate overlap between the power matrix and the sea states can be also observed for AquaBuoy (Fig. 5c), with a maximum energy power of around 50−90 kW for the most likely sea states compared to the maximum 250 kW that it would produce from H_s of 4.5–6 m and T_p of 8–13 s. Finally, higher overlap is obtained for RM5 (Fig. 5d), where the most likely sea states show powers of 100–180 kW compared to the maximum 360 kW.

3.2. WEC performance

In general, the future P_E obtained during winter is characterized by higher values offshore than near shore (Fig. 6). The WRTD shows P_E ~800−900 kW in the areas most exposed to waves and 100−400 kW in the innermost areas. Atargis is the device that will generate the greatest electrical power (~1400−1500 kW) in the entire domain. The lowest energy values will be obtained with AquaBuoy (~75 kW in the innermost areas and ~100 kW in the exposed ones). RM5 will generate around 200 kW in the western and outermost part of the study area and ~150 kW in the innermost areas. Apart from the higher or lower suitability of the devices to the different sea state ranges in which they operate, the differences among them (P_E=427 ± 248 kW, P_E=1400 ± 56 kW, P_E=89 ± 9 kW and P_E = 182 ± 13 kW, respectively) are mainly due to their different sizes (see Table 2). To prevent any dependence on the physical dimensions of the devices, an analysis in terms of dimensionless variables (power load factor, normalized capture width and operational time) was carried out.

Overall, the power load factor ε (Fig. 7) is higher for exposed areas than inner areas. The WRTD (Fig. 7a) shows low ε values, that range from around 5% for the inner areas to between 25 and 30% for the outer areas. Atargis (Fig. 7b) exhibits high ε values (around 50−60%) that can also be observed for RM5 (40−55%, Fig. 7d). AquaBuoy (Fig. 7c) shows intermediate ε values (25−40%). These results are similar to those previously described in Fig. 5, since ε depends on the ratio P_E/P_{max}, which, in turn, depends on the overlap between the power matrix and the frequency of the diferent sea states.

As for the NC_w, high values will be obtained with the WRTD (Fig. 8a), ranging from ~55 to 60% for the rias to ~45−50% for the outer areas. Moderate values (~30−50%) can be observed for Atargis (Fig. 8b) and for AquaBuoy (Fig. 8c), with NC_w values ranging from 20% to 25%. Finally, RM5 (Fig. 8d) will not be an efficient device in terms of NC_w (NC_w ~10%).

In terms of operational time, the WRTD (Fig. 9a), AquaBuoy (Fig. 9c) and RM5 (Fig. 9d) present long operational times. The WRTD (Fig. 9a) can be in working conditions ~90% of the time, although it will have a shorter operational time in the inner areas of the rias, where low waves are more frequent. Atargis (Fig. 9b) will have an operational time ranging from ~80% for external areas to ~90% when approaching the coast. AquaBuoy (Fig. 9c) will show an OT of ~95%. RM5 (Fig. 9d) can be in operation almost 100% of the time.

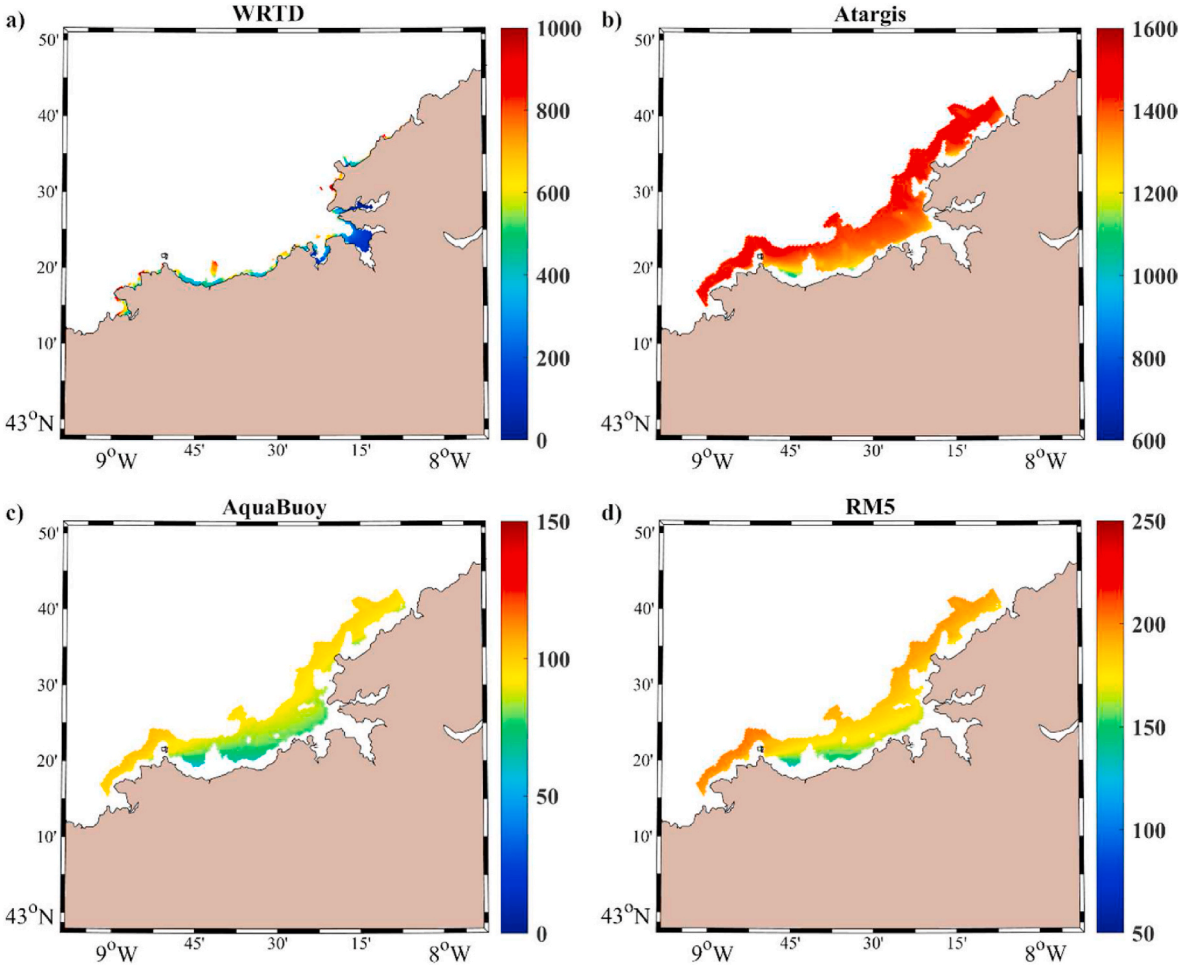

Fig. 6. Electric power output (P_E, in kW) for winter months (period between 2026 and 2045). Note the different scales.

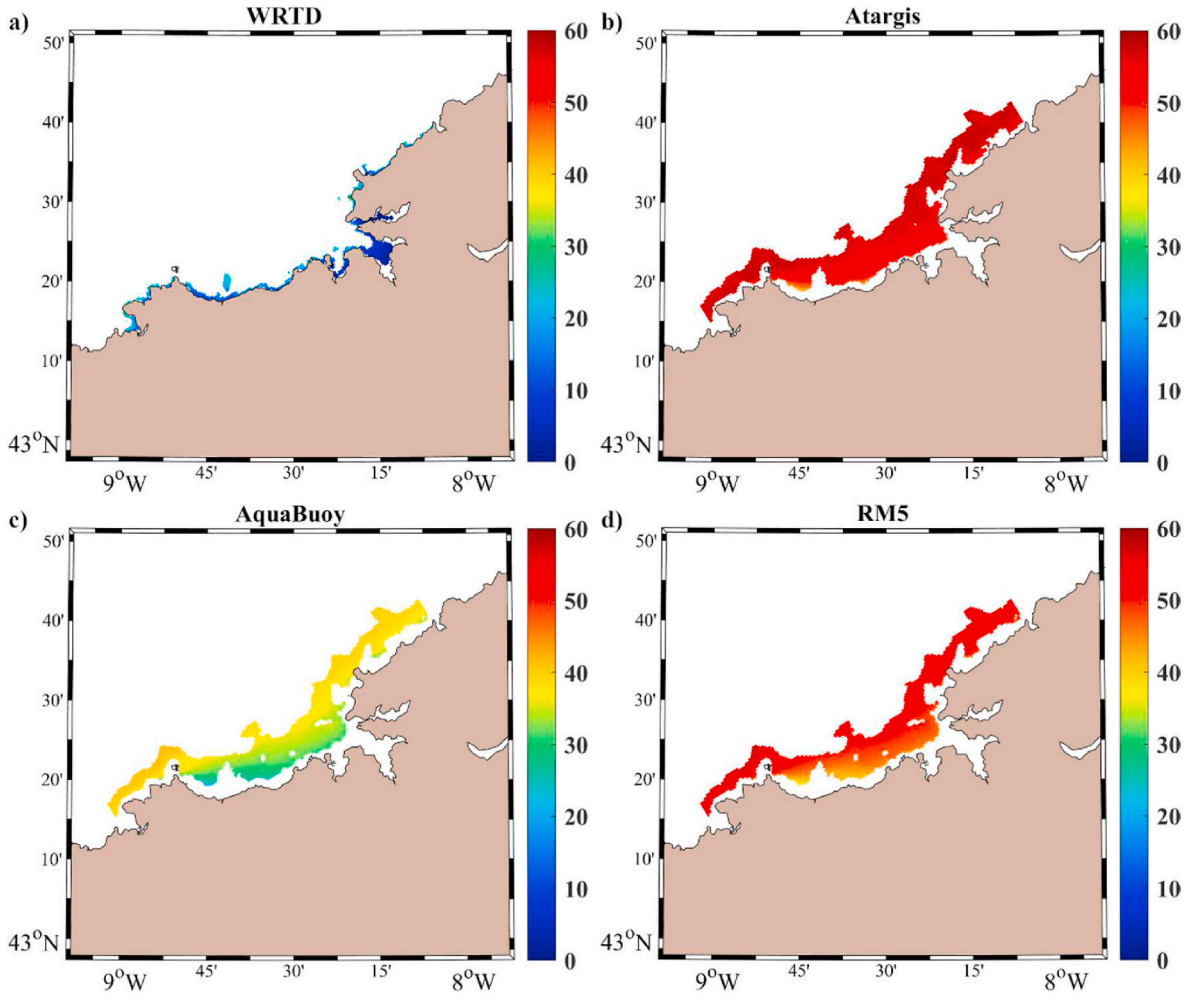

Fig. 7. Power load factor (ε, in %) for winter months (period between 2026 and 2045).

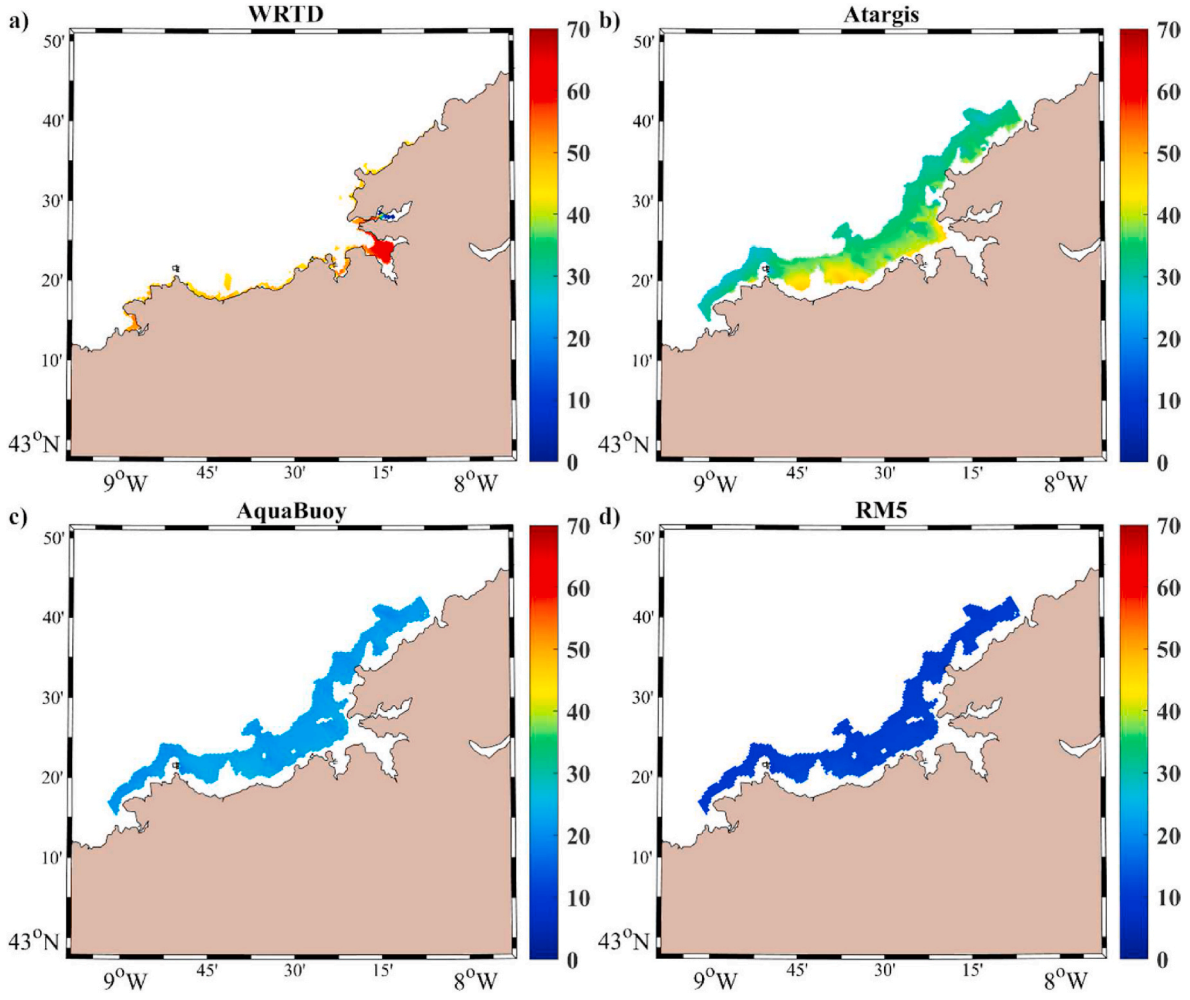

Fig. 8. Normalized capture width (NC_w, in %) for winter months (period between 2026 and 2045).

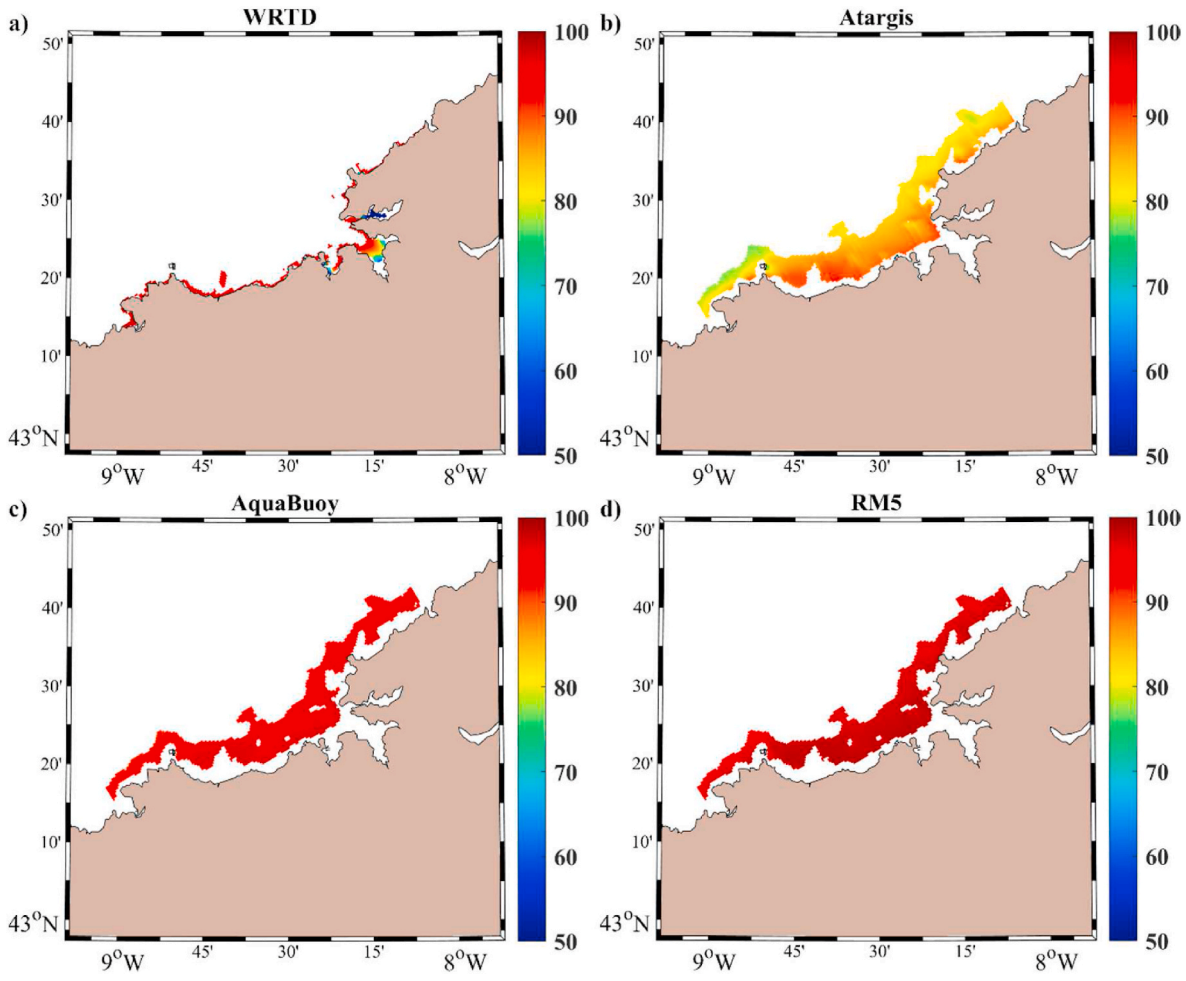

Fig. 9. Operational time (%) for winter months (period between 2026 and 2045).

4. Discussion

The present study targets to determine how the existent devices fit near future wave conditions. As three of the devices under study (Atargis, AquaBouy and RM5) can be deployed in approximately the same depths (Table 2), an intercomparison among them can help to decide which device is the best suited for the area under study. Table 3 summarizes the suitability conditions for those devices.

It can be seen that Atargis outperforms AquaBuoy and RM5 in terms of power load factor and normalized capture width, although its operational time is lower. The high *OT* provided by RM5 and AquaBuoy is due to the fact that their power matrices cover practically all the future sea states of the study area. Note that all the sea states match the RM5's power matrix and that only the smallest H_s and T_p are outside the range of AquaBuoy's. The high ε and *OT* values of RM5 make this device quite attractive for installation on the Northwest Coast of Galicia. Atargis outperforms RM5 in terms of NC_w because RM5's power matrix values are lower than Atargis', which leads to lower P_E. These values could be increased by increasing the size of RM5. However, that would lead to decrease the normalized capture width. On the other hand, AquaBuoy has an acceptable profitability size ratio and can operate most of the time, but its main drawback is its low energy conversion.

Overall, results suggest that future wave energy farms on the Northwest coast of Galicia could be made up of Atargis due to its high energy production and great suitability under near future wave climate conditions. In addition, it presents acceptable production-size profitability and operational time. This WEC operates in intermediate waters, so it could harvest wave energy at offshore locations to capture energetic waves and be close enough to reduce installation and maintenance costs. Additionally, it is a quite submerged WEC, reducing visual impact.

Table 3
Suitability of intermediate water devices for the study area. The higher the values, the more suitable the device. The error intervals represent the standard deviation calculated as described in section 2.6.

	ε (%)	NC_w(%)	*OT* (%)
Atargis	55.4 ± 2.2	35.5 ± 4.1	84.5 ± 3.3
AquaBuoy	35.7 ± 3.4	22.0 ± 0.9	95.1 ± 1.2
RM5	50.6 ± 3.59	10.8 ± 0.66	97.2 ± 0.9

AquaBuoy had been previously analized for the west coast of the Iberian Peninsula by Ribeiro et al. [1]. They obtained P_E and characterized the efficiency of this WEC by means of ε and the C_w parameters, for the same future period but considering the whole year. They obtained P_E and ε values 1.5 times lower than in the present study, where only winters, the most energetic season of the year, were considered. Table 4 summarizes the comparison between the present study and [1]. Note that [1] calculated C_w instead of NC_w, so, a size normalization was

Table 4
AquaBuoy performance comparison between the present study and [1].

WEC	Parameter	This study	Ribeiro et al. [1]
AquaBuoy	P_E (kW)	75–100	40–60
	ε (%)	25–40	15–22
	NC_w (%)	25	22

carried out for comparison in Table 4. The capture width for AquaBuoy was also analyzed by Ref. [60] in wintertime. It was found a C_w between 1.1 m and 1.4 m in nearby areas, which is equivalent to a NC_w between 18% and 23%, also consistent with our results.

As for the WRTD, this device is suited for near shore shallow waters were waves are less energetic. The device can be installed in these areas for different purposes as providing energy for aquaculture facilities and protecting them against incoming waves. Despite the device has a low power load factor (12.8 ± 7.4%), this is partially balanced by a high normalized capture width (48.9 ± 9.6%) and operational time (88.7 ± 18.9%). That means that even if the device is usually working much below its maximum performance, its efficiency in converting the available wave energy resource into electricity is high and it can work practically uninterrupted under winter conditions for some areas. However, this operational time decreases significantly in the shallowest regions because the device cannot exploit wave energy in areas where H_s is lower than 1 m. The low power load factor is due to the fact that the WRTD operates most of the time far from the H_s and T_p values corresponding to the peak of energy. As it can also be observed for Atargis, the sea states with the highest and lowest values of H_s and T_p will be excluded from the power matrix. The normalized capture width of a similar WEC (Oyster) was analyzed for the 20th century winters by Ulazia et al. in [61]. They found lower values of NC_w (between 30 and 40%) in the 20th century in Cabo Silleiro (West Coast of Galicia). Their result differs slightly from ours probably because of studying different geographic locations and sea states.

The combined use of Atargis for intermediate waters and WRTDs for shallow waters seems to be the best choice for the region under scope. The use of WRTDs is an optimal option in inner areas near harbors, where they can take advantage of the existent infrastructure to reduce impact and costs. For example, near the Outer Port of A Coruña (~43°20′N, 8°30′W, Fig. 1).

5. Conclusions and future outlook

This study characterized the wave climate for NW Spain during winter from 2026 to 2045 under the RCP8.5 scenario and analyzed the suitability to harness wave energy resource with four WECs. Wintertime was chosen because it is the season when the sea states are more energetic. The suitability to harness the wave energy resource was analyzed for three WECs that operate at intemerdiate/deep waters (Atargis, AquaBuoy and RM5) and for another one designed for shallow waters (a WaveRoller type device, WRTD). To achieve this goal, high-resolution (450 m × 450 m) significant wave height and peak period data were obtained from simulations of the third-generation SWAN model forced with the BCC-CSM1.1 m GCM wind data and outputs from the WaveWatchIII ocean model. The suitability conditions of the WECs were analyzed by means of three different parameters: power load factor, normalized capture width and operational time. These parameters take on special meaning in winter months because the energy production and WEC's efficiency will depend on how well fitted will be the power matrices to the future sea states, more energetic in wintertime.

According to the three suitability parameters and attending to the WECs designed to work in intermediate/deep waters, Atargis is the most suitable device to set up the future wave energy farms in the Northwestern Spain. For shallow waters, it was observed that the WRTD ensures high operability and efficiency. For these reasons, a combination of Atargis and WRTDs is proposed to make up the future wave energy farms on the Northwestern Spain coast.

The analysis was carried out for four devices as an example of the protocol to be followed. However, other devices, study areas, periods, seasons and climate scenarios can be chosen. The protocol we propose here consists of determining the near-future sea states to be faced by the devices and using different metrics like the power load factor, the normalized capture width and the operational time to determine the suitability of the devices for the prevalent sea states in the area. This, in turn, can help developers to adapt their devices to particular sea conditions. This protocol is applicable to any device and region worldwide.

Moreover, future studies could develop a risk assessment of a wave energy farm in the area under study, within the frame of an extreme wave analysis in the upcoming decades. It will also be interesting the use of CMIP6 data for further investigation.

Finally, it is worth mentioning that environmental, political and economic issues outside this study's scope must also be considered to choose the best location for the installation of future wave farms, as well as a seasonal variability analysis.

Author contributions

Conceptualization, B. Arguilé-Pérez, X. Costoya, A.S. Ribeiro, M. deCastro and M. Gómez-Gesteira; methodology, B. Arguilé-Pérez, X. Costoya, M. deCastro, A.S. Ribeiro and M. Gómez-Gesteira; software, B. Arguilé-Pérez and M. Gómez-Gesteira; validation, B. Arguilé-Pérez and A.S. Ribeiro; formal analysis, B. Arguilé-Pérez, X. Costoya, M. deCastro, A.S. Ribeiro and M. Gómez-Gesteira; investigation, B. Arguilé-Pérez, X. Costoya, M. deCastro, A.S. Ribeiro and M. Gómez-Gesteira; resources, M. deCastro and M. Gómez-Gesteira; data curation, B. Arguilé-Pérez, A.S. Ribeiro and M. Gómez-Gesteira; writing—original draft preparation, B. Arguilé-Pérez; writing—review and editing, M. deCastro, X. Costoya, A. S. Ribeiro and M. Gómez-Gesteira; visualization, B. Arguilé-Pérez, X. Costoya, M. deCastro, A.S. Ribeiro and M. Gómez-Gesteira; supervision, X. Costoya, M. deCastro and M. Gómez-Gesteira; project administration, M. deCastro; funding acquisition, M. deCastro. All authors have read and agreed to the published version of the manuscript.

Declaration of competing interest

The authors declare that they have no known competing financial interests or personal relationships that could have appeared to influence the work reported in this paper.

Data availability

Publicly available datasets were analyzed in this study

Acknowledgements

The authors would like to acknowledge funding from the Xunta de Galicia under project ED431C 2021/44 (Grupos de Referencia Competitiva) and the Ministry of Science and Innovation of the Government of Spain under the project SURVIWEC PID2020-113245RB-I00. This work was partially supported by Project TED2021-129479A-100 (SAFE project) funded by MCIN/AEI/10.13039/501100011033 and the "European Union NextGenerationEU/PRTR". Moreover, this study forms part of the Marine Science programme (ThinkInAzul) supported by Ministerio de Ciencia e Innovación and Xunta de Galicia with funding from European Union NextGenerationEU (PRTR-C17. I1) and European Maritime and Fisheries Fund. Thanks are also due to the Portuguese Science Foundation (FCT) FCT/MCTES for the financial support to CESAM (UIDB/50017/2020þUIDP/50017/2020), through national funds. Additionally, this study was partially supported under the SMART project funded by the AI Moonshot Challenge 2020, promoted by the Portuguese Space Agency - Portugal Space. The present study is also part of the project "WECAnet: A pan-European network for Marine Renewable Energy" (CA17105), which received funding from the HORIZON2020 Framework Programme by COST (European Cooperation in Science and Technology), a funding agency for research and innovation networks. X. Costoya is supported by Grant IJC2020-043745-I/MCIN/AEI/10.13039/501100011033 by MCIN/AEI/10.13039/501100011033 and by "European Union NextGenerationEU/PRTR". B. Arguilé-Pérez is supported by Grant PRE2021-097580 funded by MCIN/AEI/10.13039/501100011033 and by "ESF Investing in your future". Funding for open access charge: Universidade de Vigo/CISUG.

Appendix

Tables below show the power matrices for each WEC considered.

Table A1
Power matrix (in kW) for the wave energy converter WRTD, obtained from Ref. [49].

Significant Wave Height, H_s [m] \ Peak Period, T_p [s]	4	5	6	7	8	9	10	11	12	13	14	15	16
7	0	0	0	2871	3119	3131	3127	3176	3332	2877	2925	2676	2658
6.5	0	0	0	2778	3044	3001	2989	3211	2986	2896	2716	2455	2309
6	0	0	0	2406	2713	2776	2344	2705	2451	2396	2182	2414	2133
5.5	0	0	0	1979	2339	2308	2115	2389	2120	2012	1940	1518	1587
5	0	0	1247	1670	1965	1962	2097	2002	1833	1798	1814	1459	1442
4.5	0	0	1219	1408	1644	1677	1807	1641	1662	1562	1404	1370	1191
4	0	0	843	1093	1352	1427	1430	1390	1158	1224	1139	1138	863
3.5	0	0	655	934	1032	1085	1241	1075	973	925	862	747	688
3	0	368	503	693	799	824	876	792	759	704	546	579	554
2.5	0	254	378	467	568	623	616	601	519	523	481	390	428
2	75	160	233	301	380	408	383	399	329	365	319	265	259
1.5	63	92	126	168	201	213	201	239	207	198	183	150	154
1	27	39	57	76	87	104	109	100	101	98	94	94	87

Table A2
Power matrix (in kW) for the wave energy converter Atargis, obtained from Ref. [44].

Significant Wave Height, H_s [m] \ Peak Period, T_p [s]	4.5	5.5	6.5	7.5	8.5	9.5	10.5	11.5	12.5	13.5	14.5	15.5
4.498	1523	2245	2471	2443	2427	2514	2519	2495	2515	2303	2067	1911
4.152	1199	2032	2470	2467	2494	2530	2498	2513	2370	2094	1882	1743
3.806	904	1874	2492	2484	2480	2529	2506	2450	2129	1885	1698	1575
3.46	627	1695	2329	2477	2517	2517	2511	2186	1888	1676	1513	1408
3.114	0	1406	2095	2374	2472	2421	2205	1899	1646	1467	1329	1240
2.768	0	1039	1752	2073	2115	2031	1859	1612	1405	1258	1144	1072
2.422	0	711	1296	1578	1655	1628	1515	1325	1164	1049	960	904
2.076	0	0	895	1132	1223	1235	1175	1042	924	840	775	736
1.73	0	0	555	746	833	868	845	761	687	634	592	569
1.384	0	0	273	426	501	543	542	498	459	431	411	403
1.038	0	0	0	174	239	277	287	269	256	246	242	244
0.692	0	0	0	0	0	0	100	98	99	100	103	109
0.346	0	0	0	0	0	0	0	0	0	0	0	0

Table A3
Power matrix (in kW) for the wave energy converterAquaBuoy, obtained from Ref. [52].

Significant Wave Height, H_s [m] \ Peak Period, T_p [s]	5	6	7	8	9	10	11	12	13	14	15	16	17
5.5	0	0	0	250	250	250	250	250	211	172	172	172	92
5.0	0	0	0	250	250	250	250	214	175	142	142	142	77
4.5	0	0	0	223	250	239	208	173	142	115	115	115	62
4.0	0	0	0	122	176	198	188	164	137	112	91	91	49
3.5	0	0	93	135	152	144	126	105	86	70	70	70	38
3.0	0	54	68	99	111	106	92	77	63	51	51	51	27
2.5	0	37	47	69	77	73	64	54	43	36	36	36	19
2.0	0	24	30	44	49	47	41	34	28	23	23	23	12
1.5	0	13	17	25	27	26	23	19	15	12	12	12	7
1.0	0	0	8	11	12	11	10	8	7	0	0	0	0

Table A4
Power matrix (in kW) for the wave energy converter RM5, obtained from Ref. [55].

Significant Wave Height, Hs [m] \ Peak Period, Tp [s]	5.2	6.4	7.5	8.7	9.9	11.0	12.2	13.3	14.5	15.7	16.8	18.0	19.1	20.3
5.75	360	360	360	360	360	360	360	360	360	340	319	299	276	251
5.25	360	360	360	360	360	360	360	349	333	299	280	261	242	220
4.75	335	360	360	360	360	349	317	302	288	259	243	225	209	190
4.25	277	317	319	316	327	299	272	257	246	220	207	192	177	162
3.75	224	259	262	262	272	250	228	215	205	183	173	160	148	135
3.25	175	204	209	210	221	203	186	176	166	148	140	130	121	110
2.75	131	155	160	163	172	159	145	138	130	116	110	101	95	87
2.25	91	110	116	119	127	117	108	102	97	86	83	76	71	65
1.75	58	72	77	82	87	81	74	70	67	60	58	53	49	45
1.25	32	41	45	48	52	49	45	42	40	36	35	32	29	27
0.75	12	17	19	21	23	22	21	19	19	17	16	14	13	12

References

[1] Ribeiro AS, deCastro M, Rusu L, Bernardino M, Dias JM, Gomez-Gesteira M. Evaluating the future efficiency of wave energy converters along the NW coast of the iberian Peninsula. Energies 2020;13. https://doi.org/10.3390/en13143563.

[2] Guo B, Ringwood JV. A review of wave energy technology from a research and commercial perspective. IET Renew Power Gener 2021;15:3065–90.

[3] Aarnes OJ, Reistad M, Breivik Ø, Bitner–Gregersen E, Ingolf Eide L, Gramstad O, Magnusson AK, Natvig B, Vanem E. Projected changes in significant wave height toward the end of the 21st century: northeast A tlantic. J Geophys Res: Oceans 2017;122:3394–403.

[4] Bricheno LM, Wolf J. Future wave conditions of Europe, in response to high-end climate change scenarios. J Geophys Res: Oceans 2018;123:8762–91.

[5] Camus P, Losada IJ, Izaguirre C, Espejo A, Menéndez M, Pérez J. Statistical wave climate projections for coastal impact assessments. Earth's Future 2017;5:918–33.

[6] Casas-Prat M, Wang XL, Swart N. CMIP5-based global wave climate projections including the entire Arctic Ocean. Ocean Model 2018;123:66–85.

[7] Charles E, Idier D, Delecluse P, Déqué M, Le Cozannet G. Climate change impact on waves in the Bay of Biscay, France. Ocean Dynam 2012;62:831–48.

[8] Dobrynin M, Murawsky J, Yang S. Evolution of the global wind wave climate in CMIP5 experiments. Geophys Res Lett 2012;39.

[9] Hemer MA, Fan Y, Mori N, Semedo A, Wang XL. Projected changes in wave climate from a multi-model ensemble. Nat Clim Change 2013;3:471–6.

[10] Hemer MA, Katzfey J, Trenham CE. Global dynamical projections of surface ocean wave climate for a future high greenhouse gas emission scenario. Ocean Model 2013;70:221–45.

[11] Lemos G, Semedo A, Dobrynin M, Behrens A, Staneva J, Bidlot J-R, Miranda PM. Mid-twenty-first century global wave climate projections: results from a dynamic CMIP5 based ensemble. Global Planet Change 2019;172:69–87.

[12] Mori N, Yasuda T, Mase H, Tom T, Oku Y. Projection of extreme wave climate change under global warming. Hydrological Research Letters 2010;4:15–9.

[13] Perez J, Menendez M, Camus P, Mendez FJ, Losada IJ. Statistical multi-model climate projections of surface ocean waves in Europe. Ocean Model 2015;96:161–70.

[14] Semedo A, Weisse R, Behrens A, Sterl A, Bengtsson L, Günther H. Projection of global wave climate change toward the end of the twenty-first century. J Clim 2012;26:8269–88.

[15] Wang XL, Feng Y, Swail VR. Climate change signal and uncertainty in CMIP5-based projections of global ocean surface wave heights. J Geophys Res: Oceans 2015;120:3859–71.

[16] Wang XL, Feng Y, Swail VR. Changes in global ocean wave heights as projected using multimodel CMIP5 simulations. Geophys Res Lett 2014;41:1026–34.

[17] Rusu L. Evaluation of the near future wave energy resources in the Black Sea under two climate scenarios. Renew Energy 2019;142:137–46. https://doi.org/10.1016/j.renene.2019.04.092.

[18] Rusu L. A projection of the expected wave power in the Black Sea until the end of the 21st century. Renew Energy 2020;160:136–47.

[19] Alizadeh MJ, Nourani V, Kavianpour MR. A statistical framework to project wave climate and energy potential in the Caspian Sea: application of CMIP6 scenarios. Int J Environ Sci Technol 2022;19:2323–36.

[20] Goharnejad H, Nikaein E, Perrie W. Assessment of wave energy in the Persian Gulf: an evaluation of the impacts of climate change. Oceanologia 2021;63:27–39. https://doi.org/10.1016/j.oceano.2020.09.004.

[21] Ribeiro AS, deCastro M, Costoya X, Rusu L, Dias JM, Gomez-Gesteira M. A Delphi method to classify wave energy resource for the 21st century: application to the NW Iberian Peninsula. Energy 2021;235:121396. https://doi.org/10.1016/j.energy.2021.121396.

[22] Reeve DE, Chen Y, Pan S, Magar V, Simmonds DJ, Zacharioudaki A. An investigation of the impacts of climate change on wave energy generation: the

Wave Hub, Cornwall, UK. Renew Energy 2011;36:2404–13. https://doi.org/10.1016/j.renene.2011.02.020.
[23] Sierra JP, Casas-Prat M, Campins E. Impact of climate change on wave energy resource: the case of Menorca (Spain). Renew Energy 2017;101:275–85.
[24] Gleizon P, Campuzano F, Carracedo P, Martinez A, Goggins J, Atan R, Nash S. Wave energy resources along the European Atlantic coast. In: Marine renewable energy. Springer; 2017. p. 37–69.
[25] Iglesias G, López M, Carballo R, Castro A, Fraguela JA, Frigaard P. Wave energy potential in Galicia (NW Spain). Renew Energy 2009;34:2323–33. https://doi.org/10.1016/j.renene.2009.03.030.
[26] Veigas M, López M, Romillo P, Carballo R, Castro A, Iglesias G. A proposed wave farm on the Galician coast. Energy Convers Manag 2015;99:102–11.
[27] Arguilé-Pérez B, Ribeiro AS, Costoya X, deCastro M, Carracedo P, Dias JM, Rusu L, Gómez-Gesteira M. Harnessing of different WECs to harvest wave energy along the Galician coast (NW Spain). J Mar Sci Eng 2022;10. https://doi.org/10.3390/jmse10060719.
[28] Ribeiro AS, Costoya X, de Castro M, Carvalho D, Dias JM, Rocha A, Gomez-Gesteira M. Assessment of hybrid wind-wave energy resource for the NW coast of Iberian Peninsula in a climate change context. Appl Sci 2020;10:7395.
[29] Jiang H, Chen G. A global view on the swell and wind sea climate by the Jason-1 mission: a revisit. J Atmos Ocean Technol 2013;30:1833–41.
[30] IDAE. Evaluación del Potential de la Energía de las Olas. 2011.
[31] Costoya X, deCastro M, Carvalho D, Arguilé-Pérez B, Gómez-Gesteira M. Combining offshore wind and solar photovoltaic energy to stabilize energy supply under climate change scenarios: a case study on the western Iberian Peninsula. Renew Sustain Energy Rev 2022;157:112037. https://doi.org/10.1016/j.rser.2021.112037.
[32] Lira-Loarca A, Ferrari F, Mazzino A, Besio G. Future wind and wave energy resources and exploitability in the Mediterranean Sea by 2100. Appl Energy 2021;302:117492.
[33] Ribeiro AS, Lopes CL, Sousa MC, Gomez-Gesteira M, Dias JM. Flooding conditions at aveiro Port (Portugal) within the framework of projected climate change. J Mar Sci Eng 2021;9. https://doi.org/10.3390/jmse9060595.
[34] THREDDS Data Server . [WWW Document], n.d. URL http://data-cbr.csiro.au/thredds/catalog/catch_all/CMAR_CAWCR-Wave_archive/Global_wave_projections/catalog.html (accessed 5.31.22).
[35] Deltares. Delft3D-WAVE. Simulation of short-crested waves with SWAN. User Manual. Hydro-Morphodynamics 2022. https://doi.org/10.5285/e0f0bb80-ab44-2739-e053-6c86abc0289c. Version: 4.05.
[36] GEBCO Compilation Group, 2022. GEBCO_2022 Grid. https://doi.org/10.5285/e0f0bb80-ab44-2739-e053-6c86abc0289c.
[37] Beijing Climate Center. CEDA Archive [WWW Document]. WCRP CMIP5: Beijing Climate Center (BCC) bcc-csm1-1 model output for the rcp85 experiment. URL, https://catalogue.ceda.ac.uk/uuid/6f7c49351cce4daa96b6a496c09f4315. [Accessed 6 August 2020].
[38] Santos F, Gómez-Gesteira M, DeCastro M, Añel JA, Carvalho D, Costoya X, Dias JM. On the accuracy of CORDEX RCMs to project future winds over the Iberian Peninsula and surrounding ocean. Appl Energy 2018;228:289–300. https://doi.org/10.1016/j.apenergy.2018.06.086.
[39] Mota P, Pinto J. Wave energy potential along the western Portuguese coast. Renew Energy 2014;71:8–17. https://doi.org/10.1016/j.renene.2014.02.039.
[40] Cornett AM. A global wave energy resource assessment, in'proceedings of the 18th ISOPE conference'. Vancouver: BC, Canada; 2008. p. 9.
[41] Astariz S, Iglesias G. The collocation feasibility index – a method for selecting sites for co-located wave and wind farms. Renew Energy 2017;103:811–24. https://doi.org/10.1016/j.renene.2016.11.014.
[42] Stewart RH. In: Stewart Robert H, editor. Introduction to physical oceanography. Edition. Texas A&M University; 2008. September 2008.
[43] Ahamed R, McKee K, Howard I. Advancements of wave energy converters based on power take off (PTO) systems: a review. Ocean Eng 2020;204:107248. https://doi.org/10.1016/j.oceaneng.2020.107248.
[44] Siegel SG. Numerical benchmarking study of a cycloidal wave energy converter. Renew Energy 2019;134:390–405. https://doi.org/10.1016/j.renene.2018.11.041.
[45] Cheng Y, Ji C, Zhai G. Fully nonlinear analysis incorporating viscous effects for hydrodynamics of an oscillating wave surge converter with nonlinear power take-off system. Energy 2019;179:1067–81. https://doi.org/10.1016/j.energy.2019.04.189.
[46] Fanti V. Application of snl-swan model on the effect of wave farms in the wave propagation. 2019.
[47] Waveroller [WWW Document] Waveroller by AW-Energy 2022. https://aw-energy.com/waveroller/.
[48] Bozzi S, Archetti R, Passoni G. Wave electricity production in Italian offshore: a preliminary investigation. Renew Energy 2014;62:407–16. https://doi.org/10.1016/j.renene.2013.07.030.
[49] Babarit A, Hals J, Muliawan MJ, Kurniawan A, Moan T, Krokstad J. Numerical benchmarking study of a selection of wave energy converters. Renew Energy 2012;41:44–63.
[50] Siegel SG. Cycloidal wave energy converter. In: Final scientific report. United States: Atargis Energy Corporation; 2012. https://doi.org/10.2172/1061484. No. DOE/EE0003635).
[51] Atargis Energy Corporation. Atargis CycWEC [WWW Document]. URL, https://atargis.com/CycWEC.html; 2020.
[52] Silva D, Rusu E, Soares CG. Evaluation of various technologies for wave energy conversion in the Portuguese nearshore. Energies 2013;6. https://doi.org/10.3390/en6031344.
[53] Bozzi S, Besio G, Passoni G. Wave power technologies for the Mediterranean offshore: scaling and performance analysis. Coast Eng 2018;136:130–46.
[54] Zhang Y, Zhao Y, Sun W, Li J. Ocean wave energy converters: technical principle, device realization, and performance evaluation. Renew Sustain Energy Rev 2021;141:110764. https://doi.org/10.1016/j.rser.2021.110764.
[55] Yu Y-H, Jenne DS, Thresher R, Copping A, Geerlofs S, Hanna LA. Reference model 5 (RM5): oscillating Surge wave energy converter. Golden, CO: National Renewable Energy Lab.(NREL); 2015 (United States). Available on, https://www.nrel.gov/docs/fy15osti/62861.pdf.
[56] Mohtat A, Fagley C, Chitale KC, Siegel SG. Efficiency analysis of the cycloidal wave energy convertor under real-time dynamic control using a 3D radiation model. Inter Marine Energy J 2022;5:45–56.
[57] Chitale K, Fagley C, Mohtat A, Siegel S. Numerical evaluation of climate scatter performance of a cycloidal wave energy converter. International Marine Energy Journal 2022;5:315–26.
[58] Weinstein A, Fredrikson G, Parks MJ, Nielsen K. AquaBuOY - the offshore wave energy converter numerical modeling and optimization. In: Oceans '04 MTS/IEEE techno-ocean '04 (IEEE cat. No.04CH37600). Presented at the Oceans '04 MTS/IEEE techno-ocean '04. IEEE Cat. No.04CH37600); 2004. p. 1854–9. https://doi.org/10.1109/OCEANS.2004.1406425. 4.
[59] Astariz S, Iglesias G. Output power smoothing and reduced downtime period by combined wind and wave energy farms. Energy 2016;97:69–81. https://doi.org/10.1016/j.energy.2015.12.108.
[60] Rusu E. Evaluation of the wave energy conversion efficiency in various coastal environments. Energies 2014;7:4002–18. https://doi.org/10.3390/en7064002.
[61] Ulazia A, Penalba M, Ibarra-Berastegui G, Ringwood Jm, Sáenz J. Reduction of the capture width of wave energy converters due to long-term seasonal wave energy trends. Renew Sustain Energy Rev 2019;113:109267. https://doi.org/10.1016/j.rser.2019.109267.